Nanomaterial Building Blocks Based on Spider Silk–Oligonucleotide Conjugates

Martin Humenik[†,*] and Thomas Scheibel[†,‡]

[†]Lehrstuhl Biomaterialien, Fakultät für Ingenieurwissenschaften, Universität Bayreuth, Universitätsstraße 30, 95440 Bayreuth, Germany and [‡]Bayreuther Zentrum für Kolloide und Grenzflächen (BZKG), Institut für Bio-Makromoleküle (bio-mac), Bayreuther Zentrum für Molekulare Biowissenschaften (BZMB), Bayreuther Materialzentrum (BayMAT), Universität Bayreuth, Universitätsstraße 30, 95440 Bayreuth, Germany

ABSTRACT Self-assembling protein nanofibrils are promising structures for the "bottom-up" fabrication of bionanomaterials. Here, the recombinant protein eADF4(C16), a variant of *Araneus diadematus* dragline silk ADF4, which self-assembles into nanofibrils, and short oligonucleotides were modified for site-specific azide–alkyne coupling. Corresponding oligonuleotide–eADF4(C16) "click" conjugates were hybridized in linear or branched fashion according to the designed complementarities of the DNA moieties. Self-assembly properties of higher ordered structures of the spider silk–DNA conjugates were dominated by the silk component. Assembled β-sheet rich conjugate fibrils were similar in appearance to fibrils of unmodified eADF4(C16) but enabled the specific attachment of neutravidin-modified gold nanoparticles on their surface directed by complementary biotin–oligonucleotides, providing the basis for functionalization of such conjugates.

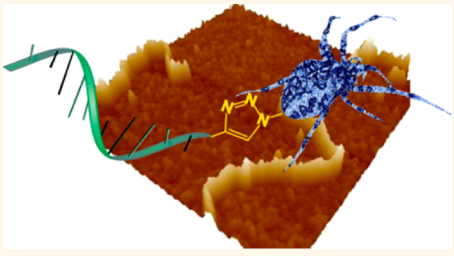

KEYWORDS: assembly · click chemistry · conjugates · fibrils · oligonucleotides · spider silk

Spider silk represents a fascinating material, since fibers of orb weaving spiders, *i.e.*, major ampullate silk, outcompete any other natural or synthetic fibrous material like nylon, Kevlar or carbon fibers in toughness.[1] Spider silk is predominantly composed of proteins, which assemble from an intrinsically unfolded and soluble state into highly aligned β-sheet rich fibrous structures.[2–4] Recombinant silk proteins, engineered on the basis of the sequence of natural spider silk, possess tunable self-organization properties,[5–7] enabling formation of different forms such as fibers,[8,9] films,[6,10,11] hydrogels,[12] capsules[5,13] and particles.[7,14] Recombinant eADF4(C16), derived from *Araneus diadematus* dragline silk ADF4,[15] also self-assembles into β-sheet rich nanofibrils[16,17] similar to cross-β fibrils of many unrelated proteins.[18] Cross-β structures share features such as the nucleation assembly mechanism *via* β-sheet hydrogen bonding,[19] perpendicular orientation of β-sheets along the fibril axis, high aspect ratios and mechanical and environmental stability.[19–21] Atomic force microscopy (AFM) indentation measurements[22,23] and statistical analysis of geometric fluctuations[24–26] have shown that Young's moduli of cross β-fibrils are in the range of 10 GPa, representing one of the most rigid proteinaceous materials.[21] Due to this mechanical stability, cross-β fibrils have become attractive scaffolds for "bottom-up" fabrication of bionanomaterials.[18,21,27]

Beyond proteins, nucleic acids are also promising materials for the construction of nanoscaled objects. DNA strands can be designed and synthesized to form tiles, *i.e.*, branched building blocks, which assemble into ordered structures *via* complementary sticky ends.[28] DNA origami even enables folding of one long single-stranded viral DNA sequence by short staple strands into highly complex structures.[29]

Covalent coupling of nucleic acids to different chemical entities, such as inorganic particles, polymers, and lipids, is widely used to expand their properties and applicability.[30–32] However, they have only rarely been furnished with peptides to create new self-assembling materials.[33] Peptide–oligonucleotide conjugates have been synthesized mainly for therapeutic reasons, *e.g.*, delivery and targeting of an antisense

* Address correspondence to martin.humenik@bm.uni-bayreuth.de.

Received for review September 20, 2013 and accepted January 9, 2014.

Published online January 09, 2014
10.1021/nn404916f

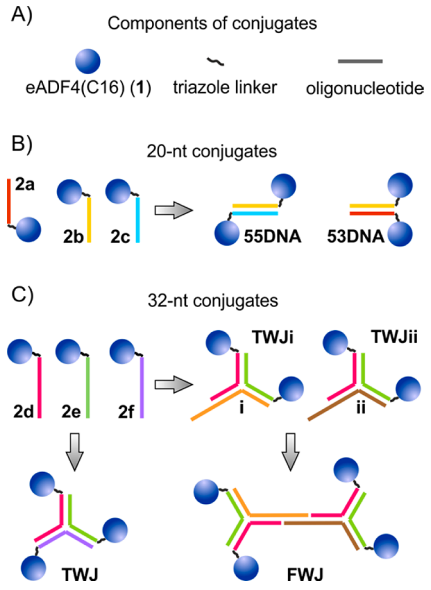

Scheme 1. Schematic representation of oligonucleotide-eADF4(C16) conjugates and hybridized constructs. (A) Components of conjugates comprising the silk moiety 1, triazole linker and oligonucleotide chain. (B) Conjugates composed of the silk moiety coupled to 3′-(2a) or 5′-(2b and c) ends of oligonucleotides comprising 20 nucleotides (nt). DNA hybrids can present eADF4(C16) on two ends (55DNA) or one end (53DNA) of the double strand. (C) Conjugates possessing the silk moiety on the 5′-end of oligonucleotides comprising 32 nt (2d–f) were designed to hybridize into branched three-way junctions (TWJ). Combining conjugates 2d, 2e and unmodified strands i or ii yielded constructs TWJi and TWJii which could assemble into four-way junctions (FWJ) *via* complementary sticky ends.

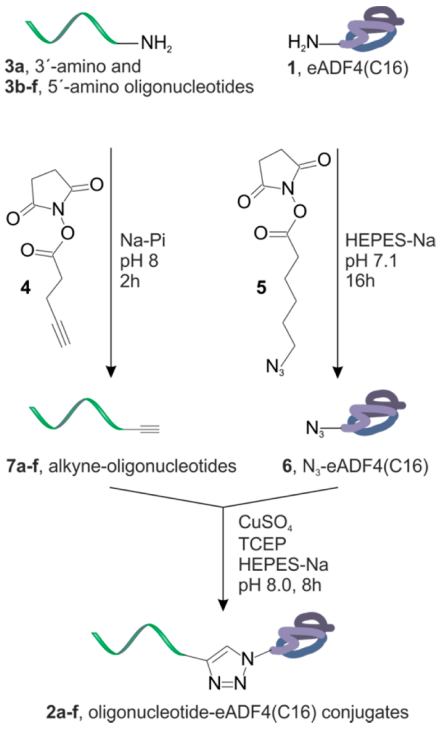

Scheme 2. Synthesis of ODN–eADF4(C16) conjugates. Alkynes 7a–f were prepared by incubating corresponding 3′-(3a) and 5′-(3b–f) amino-modified oligonucleotides with 4-pentynoic acid succinimidyl ester (4) in sodium phosphate buffer (Na-Pi), pH 8. The amino-terminus of the recombinant spider silk protein eADF4(C16) (1) was site-specifically modified with 6-azidohexanoic acid succinimidyl ester (5) in HEPES-Na buffer, pH 7.1, yielding azido modified N_3-eADF4(C16) (6). Coupling of alkynes 7a–f and the azide 6 in copper-catalyzed cycloaddition reactions provided oligonucleotide-eADF4(C16) conjugates 2a–f in HEPES-Na buffer, pH 8.

oligonucleotide into cells.[34] Additionally, functional enzymes have been coupled to oligonucleotides, and corresponding conjugates are nowadays well established in bioanalytical applications.[35] In this approach, an oligonucleotide moiety is typically attached to common mediators (streptavidine) or reporters (alkaline phosphatase, horseradish peroxidase and glucose oxidase), which are often used to visualize DNA-specific interactions.[36−38] To fabricate hierarchically structured bionanomaterials, DNA-tiles and -origami based structures were decorated using protein–oligonucleotide conjugates in order to introduce an additional functionality, *e.g.*, to provide positioning of particles with nanometer-scaled resolution.[39]

To combine the advantages of both spider silk and DNA materials, we synthesized, characterized and self-assembled novel oligonucleotide–silk conjugates. To this end, the recombinant spider silk protein eADF4(C16) and short oligodesoxynuclotides (ODNs) were site-specifically modified by an azide and an alkyne linker, respectively, for copper-catalyzed conjugation. Sequences of different oligonucleotide strands coupled with eADF4(C16) (**1**) (Scheme 1 and Table S1, Supporting Information) were designed to generate various ODN–eADF4(C16) conjugates **2a**–**f** able to form double stranded linear DNA with 5′–5′ and 5′–3′ protein moieties (**55DNA** and **53DNA**, respectively) or to generate branched motifs like three- (**TWJ**) or four-way junctions (**FWJ**).

RESULTS AND DISCUSSION

Synthesis of Oligonucleotide–Silk Conjugates. Cycloaddition reactions like copper-catalyzed or strain-promoted azide–alkyne "click" chemistry offer high chemoselectivity, which, in combination with site-specific amino acids, enables selective introduction of required labels.[40]

We used *N*-hydroxysuccinimide (NHS)-activated 6-azidohexanoic acid **5** to modify eADF4(C16) (**1**) (Scheme 2). Commonly, utilization of NHS-activated esters leads to unspecific protein labeling with little control over the sites or valency of attached labels, due to abundant primary amines, *e.g.*, originating from side chains of Lys residues.[41] Although eADF4(C16) (**1**) possesses only one reactive amine on its amino-terminus as a consequence of the specific amino acid composition,[15] the reaction resulted in increased numbers of attached azide linkers at pH 8 probably due to modification of tyrosine residues (pK_a ~10). Lowering the pH to 7.1 was required to couple ester **5** exclusively to the amino-terminus of eADF4(C16). Complete modification of eADF4(C16) was achieved after 16 h,

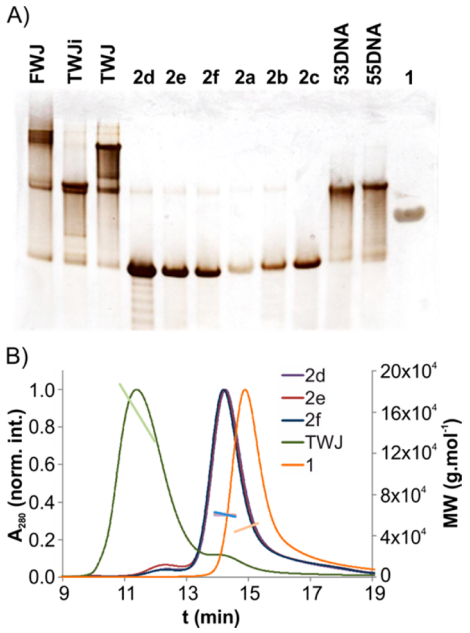

Figure 1. Analysis of synthesized ODN–eADF4(C16) conjugates. (A) Conjugates 2a–f and corresponding hybrid constructs FWJ, TWJi, TWJ, 53DNA, and 55DNA (see Scheme 1) were resolved on native-PAGE (gradient gel 4–12%, silver staining). (B) Unmodified protein eADF4(C16) (1), conjugates 2d–f and the corresponding hybridized construct TWJ were analyzed by size exclusion chromatography (SEC), and corresponding molecular weights (MW) were calculated using multiangle light scattering (MALS) (Supporting Information Table S2).

as shown by matrix-assisted laser desorption and ionization time-of-flight (MALDI-TOF) mass spectrometry analysis (Figure S1A and Table S3, Supporting Information), and site-specificity of the labeling was confirmed after glutaminase-C digest of N_3-eADF4(C16) (**6**) (Figure S1B and Table S4, Supporting Information).

Alkyne-modified oligonucleotides **7a**–**f** were prepared from corresponding commercially available amino oligonucleotides **3a**–**f** in reaction with the NHS-ester of pentynoic acid **4**, as published recently.[38] Subsequently azide–alkyne couples **6** and **7a**–**f** were conjugated in a copper-catalyzed cycloaddition in the presence of tris(2-carboxyethyl)phosphine (TCEP)[38] yielding the ODN–eADF4(C16) conjugates **2a**–**f** (Scheme 2). The reaction required the presence of 5 equiv of the azide-modified protein **6** for complete consumption of the alkyne-ODNs **7a**–**f**, as exemplarily shown for reaction mixtures comprising **6** and **7f** in different ratios by reversed-phase high pressure liquid chromatography (RP-HPLC) analysis (Supporting Information Figure S2). Conjugates **7a**–**f** were conveniently purified by anion exchange chromatography with yields of 45–60%. Purity and identity of prepared conjugates **7a**–**f** were confirmed by native-polyacrylamide gel electrophoresis (PAGE) (Figure 1A), SEC-MALS (Figure 1B), HPLC (Figure S2) and MALDI-TOF analysis (Table S5, Supporting Information).

Conjugates **2a**–**f** possess in comparison to unmodified protein **1** a lower molecular weight (MW)/charge ratio (*e.g.*, 1504 for **2a**, 1205 for **2d** and 2978 for **1**), due to highly negatively charged oligonucleotide polyphosphate chains coupled to the protein moiety. Since both unmodified protein **1** and the conjugates, showed rather comparable hydrodynamic radii (R_h ~ 5 nm; Table S2), this lower MW/charge ratio resulted in a higher mobility in native-PAGE (Figure 1A). We could exclude an influence of protein conformation on the mobility changes, since eADF4(C16) and the protein moiety in the conjugates were structurally identical (see below, Figures 4A, S4, left panel and 5A). In contrast, changing the conformation of the oligonucleotide moieties, *e.g.*, in the branched topology of **TWJ** -(Scheme 1) resulted in higher hydrodynamic radii (R_h = 9 nm, Table S2) accompanied by a significant retardation in PAGE.

Simple conjugates were further able to form less stable homodimers (weak upper bands in **2a**–**2f**, Figure 1A), yielding a mobility comparable to that of the designed heterodimers (**TWJi** or **55DNA**, Figure 1A and Scheme 1). Importantly, although the conjugates **2a**–**f** possess bulky protein heads, they successfully hybridized (Figure 1A) into linear **55DNA** and **53DNA** and into branched **TWJ** and **FWJ** constructs, according to the design presented in Scheme 1. However, less efficient association was observed for **TWJ** and **FWJ**. To accomplish hybridization of complex DNA structures, preheating of samples to 90–95 °C followed by slow cooling, to favor thermodynamically stable structures, is typically performed. Here, elevated temperatures triggered the formation of β-sheet rich structures of eADF4(C16) resulting in premature aggregation of the conjugates. Thus, only prolonged incubation at RT could be applied for the hybridization.

Self-Assembly of Oligonucleotide–Silk Conjugates. Controlled assembly of eADF4(C16), conjugates **2a**–**f**, and corresponding hybridized constructs was initiated upon addition of kosmotropic phosphate ions at room temperature. As described previously, nucleated assembly yields eADF4(C16) fibrils at low phosphate concentrations.[7,17] Morphologies of assembled conjugates **2a**–**f** hybridized linear **55DNA** and **53DNA** and branched **TWJ** and **FWJ** constructs were investigated by transmission electron microscopy (TEM) (Figure 2A,C,E) and atomic force microscopy (AFM) (Figure 2B,D,F). Remarkably, the morphology of the silk fibrils was apparently not influenced by the covalently coupled oligonucleotides. TEM images revealed that the unmodified eADF4(C16) and corresponding oligonucleotide–eADF4(C16) conjugates formed nontwisted fibrils of similar length (~1–5 μm) and diameter (~8 nm for eADF4(C16) and ~10 nm for conjugates). AFM scans revealed fibril heights of 2.5–3.0 nm (Figure S3, Supporting Information).

Formerly, fibrils prepared from unmodified eADF4(C16) exhibited X-ray diffraction patterns typical for

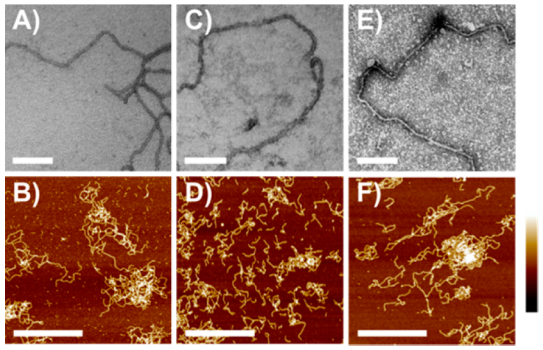

Figure 2. Characterization of fibrils assembled from unmodified eADF4(C16) and oligonucleotide–silk conjugates. (A and B) eADF4(C16) fibrils; (C and D) conjugate 2f fibrils; (E and F) TWJ fibrils. Scale bars represent 100 nm in TEM pictures (upper panel) and 2 μm in AFM height images (lower panel); color bar in the lower panel represents heights from −5 (dark) to 5 (bright) nm.

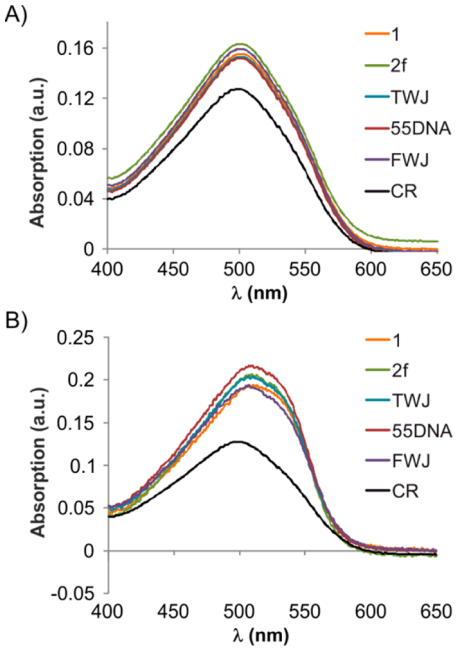

Figure 3. Congo Red spectra recorded in presence of soluble eADF4(C16) and conjugates (A) or fibrils thereof (B). Spectra in (B) were corrected for light scattering of the fibrils.

cross-β sheet structures and they were able to bind thioflavin T and Congo Red (CR).[17] To determine whether the oligonucleotide chains incorporated into assembled conjugate fibrils (Figure 2) influenced protein structure, we analyzed fibrils assembled from conjugates **2a**–**f** by CR binding experiments, Fourier transform infrared spectroscopy (FT-IR) and circular dichroism (CD) (Figures 3, 4, and 5, respectively).

As presented in Figure 3A, the soluble conjugates did not bind the dye, excluding a dye-ODN strand intercalation. Corresponding conjugate fibrils showed red-shifted CR absorption spectra (Figure 3B) clearly indicative of cross-β structure.[17] This finding was confirmed using FT-IR and CD spectroscopy (Figures 4 and 5, respectively).

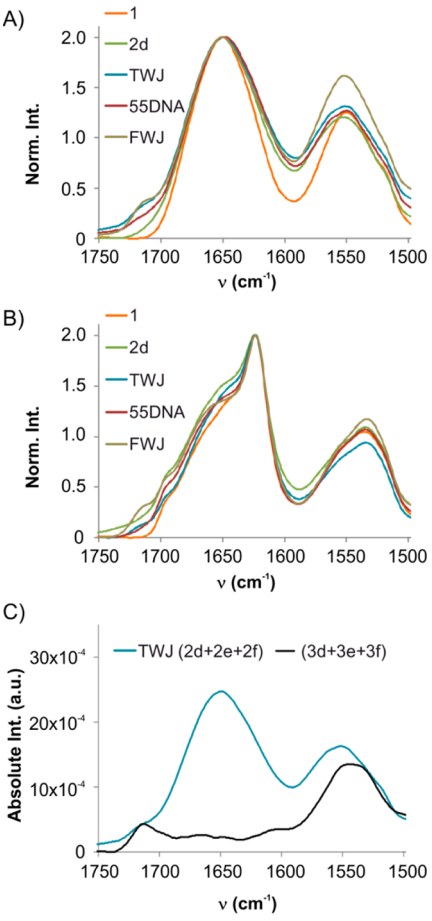

Figure 4. FT-IR spectroscopy of unmodified protein eADF4(C16) (1) and oligonucleotide–silk conjugates. Normalized Amide II and Amide I bands of soluble protein 1 and ODN–eADF4(C16) conjugates in (A) and fibrils thereof in (B). (C) Amide II and Amide I regions of the spectra of the TWJ conjugates 2d–f (20.2 μM) and of the mixture of amino-modified oligonucleotides 3d–f (46.7 μM), respectively.

FT-IR spectroscopy of peptide bond vibrations represented by Amide I (1600–1700 cm^{-1}, C=O stretching) and Amide II (1500–1580 cm^{-1}, N–H bending in combination with C–N asymmetric stretching) bands was previously established for analysis of natural[42,43] and recombinant silk proteins[5,6,44–48] as well as for cross-β structures.[49–53]

Fourier self-deconvolution (FSD) of the Amid I band for the soluble as well as the fibrous state of the unmodified protein **1** (Figure S4A,B) resulted in patterns characteristic for β-sheet (1616–1637 and 1697–1703 cm^{-1}), random coil (1638–1655 cm^{-1}), α-helical (1656–1662 cm^{-1}) and turn (1663–1696 cm^{-1}) structures.[44,48] With the use of these peak assignments, fractions of secondary structure were calculated for soluble forms of the unmodified protein **1** as well as the protein moiety of conjugates, which both consist prevalently of random coils and helices (~75%) (Table S6 and data not shown). The Amide I band in FT-IR spectra at 1650 cm^{-1} (Figure 4A) and the local minimum at 198 nm in CD spectra[54] (Figure 5A)

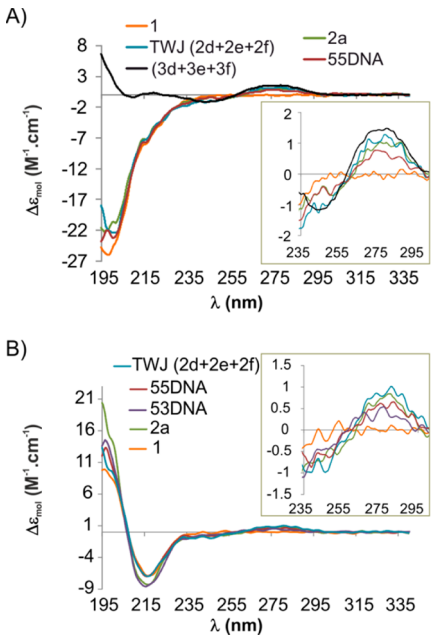

Figure 5. Far-UV CD spectra of unmodified protein eADF4-(C16) (1) and oligonucleotide−silk conjugates. (A) Soluble protein 1, corresponding conjugates and TWJ (2d−f) were compared to the mixture of amino-modified oligonucleotides 3d−f. (B) Far-UV CD spectra of corresponding fibrils. Inserts represent the spectral range (Near-UV), in which ODN chains absorb,[56] while the proteins show no strong CD signal due to the lack of tryptophan residues.

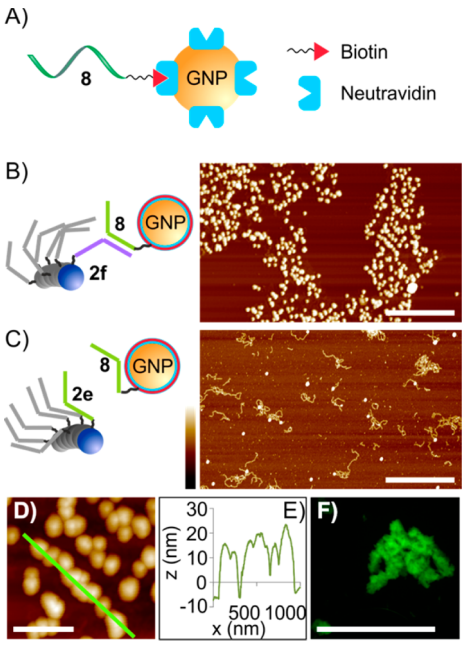

Figure 6. Immobilization of neutravidine-modified gold nanoparticles on fibrils. Cartoons in (A−C) schematically represent assembled units. 5′-Biotin-oligonucleotide 8 in (A) binds to GNPs *via* specific biotin−neutravidin interactions. Nucleic acids of 8 and 2f in (B) are complementary, whereas in (C) 8 cannot hybridize with 2e due to identical sequences. (B) The 15 nm neutravidin GNPs localized on "complementary" 2f fibrils *via* biotin−oligonucleotide 8. (C) Nonlocalized GNPs mixed with 8 and "non-complementary" 2e fibrils. (D) Cross-section of the localized GNPs (green line) and corresponding height profile in (E). (F) Entanglements of 2f fibrils labeled with fluorescein-modified oligonucleotide 9 as visualized by fluorescence light microscopy. Scale bars represent 2 μm in (B) and (C), 400 nm in (D) and 50 μm in (F). Color bar represents heights from −20 (dark) to 20 (bright) nm in (B) and (D) and −5 (dark) to 5 (bright) nm in (C).

are typical for unstructured proteins. The eADF4(C16) assembly into fibrils resulted in a clear shift of the Amide I band to 1623 cm^{-1} (Figure 4B), and FSD revealed a structural transformation toward β-sheets (~50%) (Figure S4 and Table S6). These observations could be confirmed by the position of Amide II bands[55] and the local CD minimum at 218 nm (Figure 5B).[54] FT-IR and CD spectra recorded for the simple oligonucleotide conjugates and hybridized constructs (Figures 4 and 5) were very similar to those of unmodified protein **1**. FSD (Figure S4C−F) confirmed qualitatively and quantitatively comparable secondary structure contents in these constructs. Accordingly, conjugated oligonucleotides apparently did not influence eADF4(C16) structure in solution or in fibrils, as observed in the similarities between their morphological features (Figure 2). On the basis of these structural observations, in can be assumed that the assembly mechanism of eADF4(C16)[7,17] was mostly undisturbed by the nucleic acid chains.

Spectral differences between eADF4(C16) and related conjugates, observed in Amid II bands (Figure 4), deconvoluted Amide I bands (compare Figure S4) and in CD spectra (Figure 5), arose from overlapping nucleotide and peptide signals (Figure 4C: compare **TWJ** to the mixture of amino-modified ODNs (**3d**−**f**); insert in Figure 5A: compare the black line to the other lines).

Self-assembled β-sheet rich peptide and protein fibrils represent suitable templates for "bottom-up" fabrication of biomolecular nanowires,[57,58] *e.g.*, upon metal coating,[59−61] based on their various inherent functionalities, environmental stability and exceptional mechanical properties.[21,24,62]

A specific functionalization of conjugate fibrils by gold nanoparticles (GNPs) *via* surface exposed oligonucleotides was tested in the presence of neutravidin-modified 15 nm gold nanoparticles (GNPs). The binding was mediated by 5′-biotin modified oligonucleotide **8** (Supporting Information, Table S1), which possesses a sequence identical to conjugate **2e**, and complementary to conjugates **2d** and **2f** (see Scheme 1). Oligonucleotide **8** (Figure 6A) represents a bifunctional linker, with its nucleic acid moiety enabling molecular interactions with complementary conjugate fibrils, and the biotin moiety binding GNPs *via* ligand-neutravidin interactions. In the case of "complementary" conjugate **2f**, immobilized GNPs were observed on the assembled fibrils (Figure 6B,D) using AFM. No significant binding of GNPs was observed to mica. "Non-complementary" **2e** fibrils or unmodified eADF4(C16) fibrils in combination with biotinylated strand **8** did not lead to a significant

immobilization of GNPs (Figure 6C and data not shown). To confirm these findings, 5′-fluorescein oligonucleotide **9** (Supporting Information Table S1, sequence identical to **8**) was used to label fibrils made of the complementary conjugate **2f** (Figure 6F). Again, no unspecific binding of fluorescently labeled ODN **9** to unmodified eADF4(C16) fibrils or to "non-complementary" fibrils made of conjugates **2e** was observed.

CONCLUSION

Conjugates comprising oligodesoxynucleotides and the recombinant spider silk protein eADF4(C16) were generated site-specifically using a click chemistry approach. The oligonucleotide–eADF4(C16) conjugates efficiently hybridized according to designed nucleic acids sequences arranging individual silk protein moieties in a parallel, antiparallel and in a branched fashion. Interestingly, coupled oligonucleotides did not influence the structure of the silk moiety in solution; thus, the simple conjugates and hybridized constructs retained their ability to self-assemble into β-sheet rich fibrils very similar in appearance to those of unmodified eADF4(C16). Further, fibrils prepared from the conjugates revealed surface-exposed nucleic acid chains, enabling specific attachment of neutravidin GNPs directed by hybridization of corresponding biotinylated ODNs.

Cross-β fibrils were recently successfully used as a template to align other functionalities like donor/acceptor polymers for organic solar cells,[63] fluorescent molecules for light harvesting materials[64] and enzymes to mimic long distance electron transport.[65] Here, the concept of recombinant spider silk–oligonucleotide conjugates enabled attachment of labels or functional units in a specific and reversible manner through DNA directed immobilization.[37] As shown with GNPs and fluorescently labeled oligonucleotides, the conjugate fibrils could be furnished with enzyme–oligonucleotide conjugates[38,66] to create high density enzyme arrays or cascades.

The propensity of proteins to undergo hierarchical assembly scaled over several orders of magnitudes is manifested in spider silk,[2] and a multi-level assembly was also demonstrated for cross-β fibrils.[67–69] With the toolkit presented here, formation of hierarchical fibrous arrays is feasible by designed complementarities of exposed nucleic acid chains, similarly to a recently presented approach for arranging particulate systems.[70,71]

Functional "bottom-up" assembly is typical for natural hierarchical materials and it is based on the interplay of universality and diversity.[72] Spider silks comprise only a small subset of amino acids and double stranded DNA exploits only four nucleotides. Nevertheless, diversity of functions can be reached with simple and well-analyzed building blocks using structural design, *i.e.*, defined primary sequences of biopolymers in combination with side specific chemistry.

METHODS

Preparation of Azide Modified Recombinant Spider Silk Protein N_3-eADF4(C16) (6). Recombinant protein eADF4(C16) (**1**) was prepared and purified as described previously.[15] For further modification, the protein was treated with 10 equiv of 6-azidohexanoic acid succinimidyl ester (**5**) (25 mM stock solution in DMF) in 50 mM HEPES-Na buffer, pH 7.1. The reaction mixture was incubated at room temperature (RT) for 16 h, and excess azide 5 was removed by extensive dialysis.

Preparation of Oligonucleotide–eADF4(C16) Conjugates 2a–f. Alkyl-oligonucleotides **7a**–**f** were mixed with 5 equiv of N_3-eADF4-(C16) (**6**) in 50 mM HEPES buffer, pH 8. The cycloaddition reaction was started by addition of aqueous $CuSO_4$ (2 mM) and freshly dissolved TCEP (4 mM). The reaction mixture was incubated at RT for 8 h. Conjugates **2a**–**f** were purified by anion exchange chromatography (Q-Sepharose FF, GE Healthcare, Germany) and subsequently dialyzed against 10 mM Tris/HCl, 2.5 mM EDTA, pH 8. Dialyzed solutions were centrifuged at 186 000*g* for 1 h (Optima Max-XP ultracentifuge, Beckman Coulter, Germany) and stored at 4 °C.

SEC-MALS. Size exclusion chromatography was performed using an Agilent 1100 Series HPLC system with a variable UV detector (Agilent, Germany), using a detection wavelength of 280 nm and a Superdex 200 10/300 GL column (GE Healthcare, Germany) at a flow rate of 0.8 mL/min in 25 mM Tris/HCl, 150 mM NaCl, pH 7.5. The system was additionally connected to a multiangle light scattering detector DAWN EOS (Wyatt, Germany), dynamic light scattering detector Wyatt QELS and refractive index detector Shodex RI-71 (Shodex, Germany). Molecular masses and hydrodynamic radii (R_h) from light scattering signals were calculated using the ASTRA 6 software (Wyatt, Germany).

Congo Red Binding. Spectra of Congo Red were recorded at 5 μM dye and 10 μM eADF4(C16) in 10 mM Tris/HCl, pH 8. Fibrils were prepared by incubation of unmodified eADF4(C16) (**1**) or corresponding ODN–eADF4(C16) conjugates at 15 μM in 100 mM potassium phosphate buffer (K-Pi), pH 8, for 18 h and they were subsequently dialyzed against 10 mM Tris/HCl, pH 8 before addition of the dye.

FT-IR Spectroscopy. Spectra were recorded on a Bruker Tensor 27 (Bruker, Germany) spectrometer equipped with an AquaSpec Flow Cell (microbiolytics GmbH, Germany) for acquiring FT-IR spectra in aqueous buffers. Stock solutions of conjugates **2a**–**f** in 10 mM Tris/HCl, 2.5 mM EDTA, pH 8, were used for FT-IR spectroscopy. Fibrils were prepared by incubation of the unmodified protein (**1**) and corresponding ODN–eADF4(C16) conjugates at 10 μM concentrations in 100 mM K-Pi, pH 8, for 48 h. Prepared fibrils were dialyzed against 10 mM Tris/HCl, pH 8. Absorption spectra were recorded after accumulation of 128 scans from 900 to 4000 cm^{-1}. All spectral transformations were performed using OPUS software (version 6.5, Bruker Optik, GmbH). Fourier self-deconvolution of the Amid I region (1595–1705 cm^{-1}) was performed as described previously.[44,46,47]

CD Spectroscopy. Spectra were recorded on a J-815 CD Spectrometer (Jasco, Germany) using a 0.1 cm quartz cuvette (Hellma GmbH & Co. KG, Germany). Spectra of soluble protein **1** and conjugates **2a**–**f** (3.1 μM, each) were recorded in 10 mM Tris/HCl, pH 8. Fibril assembly was initiated in 10 μM protein/conjugate solutions upon addition of 100 mM K-Pi, pH 8, and mixtures were incubated at RT for 48 h. Assembled fibrils were diluted to 3.1 μM with 10 mM Tris/HCl, pH 8.

AFM and TEM Sample Preparation. Fibrils were prepared as described in the Congo red binding experiment. For AFM analysis, 40 μL of fibril suspension was spotted on freshly

cleaved mica plates (∅ 10 mm, V1 grade, Plano GmbH, Germany), incubated for 5 min and washed four times with 50 μL of ddH_2O (Millipore). For TEM experiments, 2 μL of the fibril suspension was spotted on supports (Pioloform-carbon-coated 200-mesh copper grids (Plano GmBH, Germany), incubated for 2 min, washed with 5 μL of ddH_2O four times, and negatively stained using 5 μL of 2% uranyl acetate solution. AFM and TEM samples were allowed to dry at ambient temperature for 16 h before imaging.

Transmission Electron Microscopy. TEM imaging of dry samples was performed with a JEM-2100 transmission electron microscope (JEOL, Tokyo, Japan) operated at 80 kV. Images were recorded using a 4000 × 4000 charge-coupled device camera (UltraScan 4000; Gatan, Pleasanton, CA) and Gatan Digital Micrograph software (version 1.70.16.).

Atomic Force Microscopy. AFM scanning of dry samples was performed on a Dimension 3100 equipped with a NanoScope V controller (Veeco Instruments Inc.) operating in TappingMode using Si_3N_4 cantilevers (OMCL-AC160TS, Olympus, spring constant of 42 N/m, resonance frequency of 300 kHz, tip radius less than 7 nm). For imaging, light tapping (ratio of set point amplitude to free amplitude ~0.7−0.9) was applied. AFM scans were processed using NanoScope Analysis software Version 1.40r3 (Bruker, Santa Barbara, CA).

Binding of Neutravidin GNPs to Fibrils. Fibrils of ODN−eADF4-(C16) conjugates (10 μM, 0.23 nmol of the protein) in 100 mM K-Pi buffer, pH 8, were mixed with 5′-biotin-oligonucleotide **8** (0.3 nmol, 3.2 μL) for 1 h before neutravidin modified GNPs (30 μL) were added. This mixture was incubated for 30 min and subjected to AFM analysis.

Conflict of Interest: The authors declare no competing financial interest.

Acknowledgment. This work was supported by the Deutsche Forschungsgemeindschaft (DFG Grant No. SCHE 603/4-4). We thank C. V. Synatschke and A. Pfaffenberger for MALDI-TOF measurements, M. Heim for TEM imaging, S. Wohlrab for FSD and E. Lintz for critical comments on the manuscript.

Supporting Information Available: MALDI-TOF and RP-HPLC experiments, AFM cross sections, FSD and chemicals. This material is available free of charge *via* the Internet at http://pubs.acs.org.

REFERENCES AND NOTES

1. Gosline, J. M.; Guerette, P. A.; Ortlepp, C. S.; Savage, K. N. The Mechanical Design of Spider Silks: From Fibroin Sequence to Mechanical Function. *J. Exp. Biol.* **1999**, *202*, 3295–3303.
2. Tarakanova, A.; Buehler, M. A Materiomics Approach to Spider Silk: Protein Molecules to Webs. *JOM* **2012**, *64*, 214–225.
3. Nova, A.; Keten, S.; Pugno, N. M.; Redaelli, A.; Buehler, M. J. Molecular and Nanostructural Mechanisms of Deformation, Strength and Toughness of Spider Silk Fibrils. *Nano Lett.* **2010**, *10*, 2626–2634.
4. Gould, S. A. C.; Tran, K. T.; Spagna, J. C.; Moore, A. M. F.; Shulman, J. B. Short and Long Range Order of the Morphology of Silk from *Latrodectus hesperus* (Black Widow) as Characterized by Atomic Force Microscopy. *Int. J. Biol. Macromol.* **1999**, *24*, 151–157.
5. Rabotyagova, O. S.; Cebe, P.; Kaplan, D. L. Self-Assembly of Genetically Engineered Spider Silk Block Copolymers. *Biomacromolecules* **2009**, *10*, 229–236.
6. Krishnaji, S. T.; Bratzel, G.; Kinahan, M. E.; Kluge, J. A.; Staii, C.; Wong, J. Y.; Buehler, M. J.; Kaplan, D. L. Sequence−Structure−Property Relationships of Recombinant Spider Silk Proteins: Integration of Biopolymer Design, Processing, and Modeling. *Adv. Funct. Mater.* **2013**, *23*, 241–253.
7. Slotta, U. K.; Rammensee, S.; Gorb, S.; Scheibel, T. An Engineered Spider Silk Protein Forms Microspheres. *Angew. Chem., Int. Ed.* **2008**, *47*, 4592–4594.
8. Teulé, F.; Addison, B.; Cooper, A. R.; Ayon, J.; Henning, R. W.; Benmore, C. J.; Holland, G. P.; Yarger, J. L.; Lewis, R. V. Combining Flagelliform and Dragline Spider Silk Motifs to Produce Tunable Synthetic Biopolymer Fibers. *Biopolymers* **2012**, *97*, 418–431.
9. Xia, X. X.; Qian, Z. G.; Ki, C. S.; Park, Y. H.; Kaplan, D. L.; Lee, S. Y. Native-Sized Recombinant Spider Silk Protein Produced in Metabolically Engineered *Escherichia coli* Results in a Strong Fiber. *Proc. Natl. Acad. Sci. U. S. A.* **2010**, *107*, 14059–14063.
10. Wohlrab, S.; Müller, S.; Schmidt, A.; Neubauer, S.; Kessler, H.; Leal-Egaña, A.; Scheibel, T. Cell Adhesion and Proliferation on RGD-Modified Recombinant Spider Silk Proteins. *Biomaterials* **2012**, *33*, 6650–6659.
11. Gomes, S. C.; Leonor, I. B.; Mano, J. F.; Reis, R. L.; Kaplan, D. L. Antimicrobial Functionalized Genetically Engineered Spider Silk. *Biomaterials* **2011**, *32*, 4255–4266.
12. Schacht, K.; Scheibel, T. Controlled Hydrogel Formation of a Recombinant Spider Silk Protein. *Biomacromolecules* **2011**, *12*, 2488–2495.
13. Blüm, C.; Nichtl, A.; Scheibel, T. Spider Silk Capsules as Protective Reaction Containers for Enzymes. *Adv. Funct. Mater.* **2013**, 10.1002/adfm.201302100.
14. Numata, K.; Reagan, M. R.; Goldstein, R. H.; Rosenblatt, M.; Kaplan, D. L. Spider Silk-Based Gene Carriers for Tumor Cell-Specific Delivery. *Bioconjugate Chem.* **2011**, *22*, 1605–1610.
15. Huemmerich, D.; Helsen, C. W.; Quedzuweit, S.; Oschmann, J.; Rudolph, R.; Scheibel, T. Primary Structure Elements of Spider Dragline Silks and Their Contribution to Protein Solubility. *Biochemistry* **2004**, *43*, 13604–13612.
16. Rammensee, S.; Huemmerich, D.; Hermanson, K. D.; Scheibel, T.; Bausch, A. R. Rheological Characterization of Hydrogels Formed by Recombinantly Produced Spider Silk. *Appl. Phys. A: Mater. Sci. Process.* **2006**, *82*, 261–264.
17. Slotta, U.; Hess, S.; Spiess, K.; Stromer, T.; Serpell, L.; Scheibel, T. Spider Silk and Amyloid Fibrils: A Structural Comparison. *Macromol. Biosci.* **2007**, *7*, 183–188.
18. Cherny, I.; Gazit, E. Amyloids: Not Only Pathological Agents but Also Ordered Nanomaterials. *Angew. Chem., Int. Ed.* **2008**, *47*, 4062–4069.
19. Eichner, T. Radford, Sheena E. A Diversity of Assembly Mechanisms of a Generic Amyloid Fold. *Mol. Cell* **2011**, *43*, 8–18.
20. Jahn, T. R.; Makin, O. S.; Morris, K. L.; Marshall, K. E.; Tian, P.; Sikorski, P.; Serpell, L. C. The Common Architecture of Cross-B Amyloid. *J. Mol. Biol.* **2010**, *395*, 717–727.
21. Knowles, T. P. J.; Buehler, M. J. Nanomechanics of Functional and Pathological Amyloid Materials. *Nat. Nanotechnol.* **2011**, *6*, 469–479.
22. Kol, N.; Adler-Abramovich, L.; Barlam, D.; Shneck, R. Z.; Gazit, E.; Rousso, I. Self-Assembled Peptide Nanotubes Are Uniquely Rigid Bioinspired Supramolecular Structures. *Nano Lett.* **2005**, *5*, 1343–1346.
23. Smith, J. F.; Knowles, T. P. J.; Dobson, C. M.; MacPhee, C. E.; Welland, M. E. Characterization of the Nanoscale Properties of Individual Amyloid Fibrils. *Proc. Natl. Acad. Sci. U. S. A.* **2006**, *103*, 15806–15811.
24. Knowles, T. P.; Fitzpatrick, A. W.; Meehan, S.; Mott, H. R.; Vendruscolo, M.; Dobson, C. M.; Welland, M. E. Role of Intermolecular Forces in Defining Material Properties of Protein Nanofibrils. *Science* **2007**, *318*, 1900–1903.
25. Adamcik, J.; Jung, J.-M.; Flakowski, J.; De Los Rios, P.; Dietler, G.; Mezzenga, R. Understanding Amyloid Aggregation by Statistical Analysis of Atomic Force Microscopy Images. *Nat. Nanotechnol.* **2010**, *5*, 423–428.
26. Sachse, C.; Grigorieff, N.; Fändrich, M. Nanoscale Flexibility Parameters of Alzheimer Amyloid Fibrils Determined by Electron Cryo-Microscopy. *Angew. Chem., Int. Ed.* **2010**, *49*, 1321–1323.
27. Scheibel, T. Protein Fibers as Performance Proteins: New Technologies and Applications. *Curr. Opin. Biotechnol.* **2005**, *16*, 427–433.
28. Seeman, N. C. Nucleic Acid Nanostructures and Topology. *Angew. Chem., Int. Ed.* **1998**, *37*, 3220–3238.
29. Rothemund, P. W. K. Folding DNA to Create Nanoscale Shapes and Patterns. *Nature* **2006**, *440*, 297–302.

30. Cutler, J. I.; Auyeung, E.; Mirkin, C. A. Spherical Nucleic Acids. *J. Am. Chem. Soc.* **2012**, *134*, 1376–1391.
31. Kedracki, D.; Safir, I.; Gour, N.; Ngo, K.; Vebert-Nardin, C. DNA–Polymer Conjugates: From Synthesis, through Complex Formation and Self-Assembly to Applications. In *Bio-Synthetic Polymer Conjugates*; Schlaad, H., Ed.; Springer: Berlin Heidelberg, 2013; Vol. 253, pp 115–149.
32. Kwak, M.; Herrmann, A. Nucleic Acid/Organic Polymer Hybrid Materials: Synthesis, Superstructures, and Applications. *Angew. Chem., Int. Ed.* **2010**, *49*, 8574–8587.
33. Gour, N.; Kedracki, D.; Safir, I.; Ngo, K. X.; Vebert-Nardin, C. Self-Assembling DNA-Peptide Hybrids: Morphological Consequences of Oligonucleotide Grafting to a Pathogenic Amyloid Fibrils Forming Dipeptide. *Chem. Commun.* **2012**, *48*, 5440–5442.
34. Juliano, R. L.; Ming, X.; Nakagawa, O. The Chemistry and Biology of Oligonucleotide Conjugates. *Acc. Chem. Res.* **2012**, *45*, 1067–1076.
35. Drummond, T. G.; Hill, M. G.; Barton, J. K. Electrochemical DNA Sensors. *Nat. Biotechnol.* **2003**, *21*, 1192–1199.
36. Teller, C.; Willner, I. Organizing Protein-DNA Hybrids as Nanostructures with Programmed Functionalities. *Trends Biotechnol.* **2010**, *28*, 619–628.
37. Niemeyer, C. M. Semisynthetic DNA–Protein Conjugates for Biosensing and Nanofabrication. *Angew. Chem., Int. Ed.* **2010**, *49*, 1200–1216.
38. Humenik, M.; Huang, Y.; Wang, Y.; Sprinzl, M. C-Terminal Incorporation of Bio-Orthogonal Azide Groups into a Protein and Preparation of Protein-Oligodeoxynucleotide Conjugates by Cu(I)-Catalyzed Cycloaddition. *ChemBioChem* **2007**, *8*, 1103–1106.
39. Saccà, B.; Niemeyer, C. M. DNA Origami: The Art of Folding DNA. *Angew. Chem., Int. Ed.* **2012**, *51*, 58–66.
40. Sletten, E. M.; Bertozzi, C. R. Bioorthogonal Chemistry: Fishing for Selectivity in a Sea of Functionality. *Angew. Chem., Int. Ed.* **2009**, *48*, 6974–6998.
41. Thordarson, P.; Le Droumaguet, B.; Velonia, K. Well-Defined Protein-Polymer Conjugates-Synthesis and Potential Applications. *Appl. Microbiol. Biotechnol.* **2006**, *73*, 243–254.
42. Dicko, C.; Knight, D.; Kenney, J. M.; Vollrath, F. Secondary Structures and Conformational Changes in Flagelliform, Cylindrical, Major, and Minor Ampullate Silk Proteins. Temperature and Concentration Effects. *Biomacromolecules* **2004**, *5*, 2105–2115.
43. Papadopoulos, P.; Ene, R.; Weidner, I.; Kremer, F. Similarities in the Structural Organization of Major and Minor Ampullate Spider Silk. *Macromol. Rapid Commun.* **2009**, *30*, 851–857.
44. Hu, X.; Kaplan, D.; Cebe, P. Determining Beta-Sheet Crystallinity in Fibrous Proteins by Thermal Analysis and Infrared-Spectroscopy. *Macromolecules* **2006**, *39*, 6161–6170.
45. Slotta, U.; Tammer, M.; Kremer, F.; Koelsch, P.; Scheibel, T. Structural Analysis of Spider Silk Films. *Supramol. Chem.* **2006**, *18*, 465–471.
46. Lammel, A. S.; Hu, X.; Park, S. H.; Kaplan, D. L.; Scheibel, T. R. Controlling Silk Fibroin Particle Features for Drug Delivery. *Biomaterials* **2010**, *31*, 4583–4591.
47. Spiess, K.; Ene, R.; Keenan, C. D.; Senker, J.; Kremer, F.; Scheibel, T. Impact of Initial Solvent on Thermal Stability and Mechanical Properties of Recombinant Spider Silk Films. *J. Mater. Chem.* **2011**, *21*, 13594–13604.
48. Huang, W.; Krishnaji, S.; Hu, X.; Kaplan, D.; Cebe, P. Heat Capacity of Spider Silk-Like Block Copolymers. *Macromolecules* **2011**, *44*, 5299–5309.
49. Lee, J. S.; Park, C. B. Microfluidic Dissociation and Clearance of Alzheimer's β-Amyloid Aggregates. *Biomaterials* **2010**, *31*, 6789–6795.
50. Calero, M.; Gasset, M. Featuring Amyloids with Fourier Transform Infrared and Circular Dichroism Spectroscopies. In *Amyloid Proteins*; Sigurdsson, E. M., Calero, M., Gasset, M., Eds.; Humana Press: Totowa, NJ, 2012; Vol. 849, pp 53–68.
51. Ridgley, D. M.; Ebanks, K. C.; Barone, J. R. Peptide Mixtures Can Self-Assemble into Large Amyloid Fibers of Varying Size and Morphology. *Biomacromolecules* **2011**, *12*, 3770–3779.
52. Shaw, C. P.; Middleton, D. A.; Volk, M.; Lévy, R. Amyloid-Derived Peptide Forms Self-Assembled Monolayers on Gold Nanoparticle with a Curvature-Dependent β-Sheet Structure. *ACS Nano* **2012**, *6*, 1416–1426.
53. Williams, R. J.; Smith, A. M.; Collins, R.; Hodson, N.; Das, A. K.; Ulijn, R. V. Enzyme-Assisted Self-Assembly under Thermodynamic Control. *Nat. Nanotechnol.* **2009**, *4*, 19–24.
54. Kelly, S. M.; Jess, T. J.; Price, N. C. How to Study Proteins by Circular Dichroism. *Biochim. Biophys. Acta, Proteins Proteomics* **2005**, *1751*, 119–139.
55. Matsumoto, A.; Chen, J.; Collette, A. L.; Kim, U. J.; Altman, G. H.; Cebe, P.; Kaplan, D. L. Mechanisms of Silk Fibroin Sol-Gel Transitions. *J. Phys. Chem. B* **2006**, *110*, 21630–21638.
56. Kypr, J.; Kejnovská, I.; Renčiuk, D.; Vorlíčková, M. Circular Dichroism and Conformational Polymorphism of DNA. *Nucleic Acids Res.* **2009**, *37*, 1713–1725.
57. Lakshmanan, A.; Zhang, S.; Hauser, C. A. E. Short Self-Assembling Peptides as Building Blocks for Modern Nanodevices. *Trends Biotechnol* **2012**, *30*, 155–165.
58. Bjork, P.; Herland, A.; Hamedi, M.; Inganas, O. Biomolecular Nanowires Decorated by Organic Electronic Polymers. *J. Mater. Chem.* **2010**, *20*, 2269–2276.
59. Sakai, H.; Watanabe, K.; Asanomi, Y.; Kobayashi, Y.; Chuman, Y.; Shi, L.; Masuda, T.; Wyttenbach, T.; Bowers, M. T.; Uosaki, K.; Sakaguchi, K. Formation of Functionalized Nanowires by Control of Self-Assembly Using Multiple Modified Amyloid Peptides. *Adv. Funct. Mater.* **2013**, *23*, 4881–4887.
60. Scheibel, T.; Parthasarathy, R.; Sawicki, G.; Lin, X. M.; Jaeger, H.; Lindquist, S. L. Conducting Nanowires Built by Controlled Self-Assembly of Amyloid Fibers and Selective Metal Deposition. *Proc. Natl. Acad. Sci. U. S. A.* **2003**, *100*, 4527–4532.
61. Reches, M.; Gazit, E. Casting Metal Nanowires within Discrete Self-Assembled Peptide Nanotubes. *Science* **2003**, *300*, 625–627.
62. Makin, O. S.; Serpell, L. C. Structures for Amyloid Fibrils. *FEBS J.* **2005**, *272*, 5950–5961.
63. Barrau, S.; Zhang, F.; Herland, A.; Mammo, W.; Andersson, M. R.; Inganas, O. Integration of Amyloid Nanowires in Organic Solar Cells. *Appl. Phys. Lett.* **2008**, *93*, 023307-1–023307-3.
64. Channon, K. J.; Devlin, G. L.; MacPhee, C. E. Efficient Energy Transfer within Self-Assembling Peptide Fibers: A Route to Light-Harvesting Nanomaterials. *J. Am. Chem. Soc.* **2009**, *131*, 12520–12521.
65. Baldwin, A. J.; Bader, R.; Christodoulou, J.; MacPhee, C. E.; Dobson, C. M.; Barker, P. D. Cytochrome Display on Amyloid Fibrils. *J. Am. Chem. Soc.* **2006**, *128*, 2162–2163.
66. Wilner, O. I.; Weizmann, Y.; Gill, R.; Lioubashevski, O.; Freeman, R.; Willner, I. Enzyme Cascades Activated on Topologically Programmed DNA Scaffolds. *Nat. Nanotechnol.* **2009**, *4*, 249–254.
67. Knowles, T. P. J.; Oppenheim, T. W.; Buell, A. K.; Chirgadze, D. Y.; Welland, M. E. Nanostructured Films from Hierarchical Self-Assembly of Amyloidogenic Proteins. *Nat. Nanotechnol.* **2010**, *5*, 204–207.
68. Reches, M.; Gazit, E. Controlled Patterning of Aligned Self-Assembled Peptide Nanotubes. *Nat. Nanotechnol.* **2006**, *1*, 195–200.
69. Ridgley, D. M.; Barone, J. R. Evolution of the Amyloid Fiber over Multiple Length Scales. *ACS Nano* **2012**, *7*, 1006–1015.
70. Park, S. Y.; Lytton-Jean, A. K. R.; Lee, B.; Weigand, S.; Schatz, G. C.; Mirkin, C. A. DNA-Programmable Nanoparticle Crystallization. *Nature* **2008**, *451*, 553–556.
71. Cigler, P.; Lytton-Jean, A. K. R.; Anderson, D. G.; Finn, M. G.; Park, S. Y. DNA-Controlled Assembly of a NaTl Lattice Structure from Gold Nanoparticles and Protein Nanoparticles. *Nat. Mater.* **2010**, *9*, 918–922.
72. Buehler, M. J. Tu(r)ning Weakness to Strength. *Nano Today* **2010**, *5*, 379–383.